The two-component system ChvGI maintains cell envelope homeostasis in *Caulobacter crescentus*

Alex Quintero-Yanes[1], Jérôme Coppine[1, $], Aurélie Mayard[1] and Régis Hallez[1,2,#]

[1] *Bacterial Cell cycle & Development (BCcD), Biology of Microorganisms Research Unit (URBM), Namur Research Institute for Life Science (NARILIS), University of Namur, Namur (5000), Belgium*

[2] *WELBIO, University of Namur, Namur (5000), Belgium*

[$] *Present address: Syngulon SA, Seraing, Belgium*

[#]Corresponding author: Tel: +32 81 724 244; E-mail: regis.hallez@unamur.be

Running title: ChvGI-dependent cell envelope homeostasis

Key words: Two-component system, cell envelope, PBP, peptidoglycan, osmotic shock, mecillinam, vancomycin

Abstract

Two-component signal transduction systems (TCS) are often used by bacteria to rapidly assess and respond to environmental changes. ChvG/ChvI is a TCS conserved in α-proteobacteria and known for regulating expression of genes related to exopolysaccharide production, virulence and growth. The sensor kinase ChvG autophosphorylates upon yet unknown signals and phosphorylates the response regulator ChvI to activate transcription. Recent studies in *Caulobacter crescentus* showed that *chv* mutants are sensitive to vancomycin treatment and fail to grow in synthetic minimal media. In this work, we identified the osmotic imbalance as the main cause of growth impairment in synthetic minimal media. We also determined the ChvI regulon and confirmed that ChvI regulates cell envelope architecture at different levels by controlling outer membrane, peptidoglycan assembly/recycling and inner membrane proteins. Furthermore, we identified genes with osmoregulatory properties and confirmed that osmotic upshift is a signal triggering ChvG-dependent phosphorylation of ChvI. In addition, we challenged *chv* mutants with other cell envelope related stress and found that targeting with antibiotics the transpeptidation of peptidoglycan during cell elongation impairs growth of the mutant. Moreover, these antibiotics activate expression of the *chvIG-hprK* operon in ChvI-dependent and independent ways. Finally, we observed that the sensor kinase ChvG fused to a fluorescent protein relocates from a patchy-spotty distribution to distinctive foci after transition from complex to synthetic minimal media. Interestingly, this pattern of (re)location has been described for proteins involved in cell growth control and peptidoglycan synthesis upon osmotic shock. Overall, our data support that the ChvGI

43 TCS is mainly used to maintain cell envelope homeostasis by monitoring osmotic
44 imbalances and damages in the peptidoglycan layer.
45

Introduction

Two-component systems (TCS) equip cells with a rapid sensing and response mechanism to optimise survival in changing and stressful environments. The first component of canonical TCS, a sensor histidine kinase (HK), autophosphorylates upon input signal detection on a conserved histidine residue using the gamma-phosphoryl group of ATP. Thereafter, the HK phosphorylates a conserved aspartate residue of the second component of TCS, a cognate response regulator (RR). In most cases, the RR harbours an output domain that binds to DNA upon phosphorylation to either activate or repress transcription of target genes (Stock *et* al., 2000; Goulian. 2010; Capra & Laub. 2012). On the other hand, HKs can also exert specific phosphatase activities on their RRs to turn off the response in absence of the input signal (Gao and Stock. 2009; TuAnh and Stewart. 2011).

The Chv (**ch**romosomal **v**irulence factor) TCS conserved in α-proteobacteria and composed of the HK ChvG and the RR ChvI, was first reported as a pathogenic regulator in *Agrobacterium tumefaciens* responding to acid stress (Mantis & Winans. 1993; Li *et al.,* 2002). A study in *Sinorhizobium meliloti* showed that the ChvG homologue ExoS is negatively regulated by the periplasmic protein ExoR (Chen *et al.,* 2008). Further research in *A. tumefaciens* showed that low pH triggers ExoR proteolysis to derepress ChvG/ChvI activity (Wu *et al.,* 2012). ExoR orthologs are absent in other α-proteobacteria, such as in the animal intracellular pathogen *Brucella abortus* and the aquatic free-living bacterium *Caulobacter crescentus* (Castillo-Zéledon *et al.,* 2021; Stein *et al.,* 2021). Nonetheless, the ChvGI-dependent response to acidic conditions seems to be conserved. For instance, the ChvI homologue BvrR

in *B. abortus* is phosphorylated in combination of low pH and nutrient depletion conditions, which mimics post-infection conditions (Altamirano-Silva *et al.,* 2018).

In *C. crescentus*, ChvGI activates the expression of the small non-coding RNA (sRNA) ChvR when exposed to acidic stress or DNA damage with mitomycin C, or when cultured in synthetic minimal media (Frölich *et al.,* 2018). Once produced, ChvR subsequently inhibits translation of the TonB-dependent receptor (TBDR) ChvT (Frölich *et al.,* 2018). Interestingly, inactivating of *chvR* or *chvIG* sensitises *C. crescentus* cells to vancomycin treatment whereas a *chvT* mutant makes them resistant to this antibiotic, which suggests that vancomycin passes through the outer membrane via ChvT to reach the periplasm (Vallet *et al.,* 2020). In addition, a *chvIG* knock-out (Δ*chvIG*) mutant could not propagate in synthetic minimal media when cells are inoculated at low density, while inactivating *chvT* in a Δ*chvIG* background partially restored growth (Stein *et al.,* 2021). Although *chvIG* mutants are sensitive to acid stress when grown in minimal media, the primary cause for the growth defect has not been determined.

ChvGI is also known in *C. crescentus* to coordinate its regulation with another TCS, NtrYX, which is under control of the periplasmic protein NtrZ (Stein *et al.,* 2021). NtrZ has been only described in *C. crescentus*, while the HK NtrY and RR NtrX are known for regulating multiple processes in α-proteobacteria such as nitrogen metabolism, motility, virulence and cell envelope integrity (Pawloski *et al.,* 1991; Carrica *et al.,* 2012; Wang, D *et al.,* 2013; Lemmer *et al.,* 2020). Stein *et al.* (2021) showed that both ChvI and NtrX networks significantly overlap and these RRs have opposite regulatory functions in minimal media. For instance, while ChvI acts as a positive regulator of growth, NtrY inhibits growth. Interestingly, repression of growth in synthetic media is

caused by unphosphorylated NtrX, so that inactivating *ntrX* in a Δ*chvI* background also partially restored growth. Actually, NtrY acts as a phosphatase over the phosphorylated NtrX (NtrX~P), while NtrZ inhibits NtrY to presumably maintain high NtrX~P levels.

Here we show that *chvIG* mutants are greatly impacted due to osmotic imbalances in minimal media, but also in complex media supplemented with osmolytes. In agreement with previous data (Stein *et al.,* 2021), deletion of *chvT* and *ntrX* restored growth in hypertonic conditions. We provide a ChvI regulon, using ChIP-seq with polyclonal anti-ChvI antibodies and RNA-seq, which unveiled new targets related to peptidoglycan synthesis and recycling. We also showed that (i) ChvI is phosphorylated upon osmotic shock in a ChvG-dependent way and (ii) expression of the *chvIG-hprK* operon is induced upon treatment with antibiotics. Overall, our results confirm that the ChvGI TCS senses and responds to cell envelope stress by inducing expression of multiple genes related to cell morphology and envelope homeostasis.

Methods

Bacterial strains and growth conditions.

Strains, plasmids and oligonucleotides used in this study are listed in supplementary tables 1, 2 and 3. Plasmid construction details are presented in supplementary methods. *E. coli* strains were grown aerobically in either LB (broth) sigma or LB + 1.5% agar at 37 ºC. All *C. crescentus* strains in this study are derived of the NA1000 wild-type strain, and growth was achieved at 30 ºC in aerated conditions using either complex medium Peptone Yeast Extract (PYE) or synthetic media supplemented with glucose (M2G or M5GG) as already described in (Ronneau et al., 2016). M2G and M5GG were prepared using M2 (12.25 mM Na_2HPO_4, 7.75 mM KH_2PO_4, 9.35 mM NH_4Cl) and M5 (10 mM PIPES pH 7.2, 1 mM NaCl, 1 mM KCl, 0.37 mM Na_2HPO_4, 0.23 mM KH_2PO_4) salts, respectively, and both supplemented with (0.5 mM $MgSO_4$, 0.5 mM $CaCl_2$, 0.01 mM $FeSO_4$, 0.2% glucose). 1 mM glutamate sodium was added to make M5GG. Modified M2G 0% (Na^+, K^+), M2G 25% (Na^+, K^+) and M2G 50% (Na^+, K^+) were prepared without Na_2HPO_4 and KH_2PO_4 or either 50% or 25% of the Na_2HPO_4 and KH_2PO_4 concentrations in M2G, respectively. *C. crescentus* was grown on plates using either PYE or M2G with 1.5% agar at 30 ºC. Growth was monitored measuring OD_{660} in liquid cultures using an automated plate reader (Biotek, Epoch 2) with continuous shaking at 30 ºC. Gene expression under the control of inducible promoter (P_{xylX}) was induced either with 0.1 % D(+)-xylose (Sigma). Expression of enhanced green fluorescent protein (*egfp*) and monomeric cherry *mcherry* protein fusions was induced in fresh exponentially growing cultures ($OD_{660} \sim 0.1$) for 1 h and 4 h. Generalized transduction was performed with phage ϕCr30 according to the procedure described in (Ely, 1991). Antibiotics for *E. coli* were used with the following

final concentrations (μg ml^{-1}, in liquid/ solid medium) ampicillin (50/100), kanamycin (30/50), oxytetracycline (12.5/12.5), chloramphenicol (30/20) and for *C. crescentus* kanamycin (5/20), oxytetracycline (1/2.5), mecillinam (100/100), A22 (2.5,5) where appropriate. Plasmid delivery into *C. crescentus* was achieved by either bi- or tri-parental mating using *E. coli* S17-1 and *E. coli* MT607 as helper strains, respectively. In-frame deletions were created by using the pNPTS138-derivative plasmids as follows. Integration of the plasmids in the *C. crescentus* genome after single homologous recombination were selected on PYE plates supplemented with kanamycin. Three independent recombinant clones were inoculated in PYE medium without kanamycin and incubated overnight at 30 °C. Then, dilutions were spread on PYE plates supplemented with 3% sucrose and incubated at 30 °C. Single colonies were picked and transferred onto PYE plates with and without kanamycin. Finally, to discriminate between mutated and wild-type loci, kanamycin-sensitive clones were tested by PCR on colony using locus-specific oligonucleotides.

Spotting assays

Ten-fold serial dilutions (in PYE) were prepared in 96-well plates from 5 ml cultures in standard glass tubes grown overnight at 30 °C in the corresponding media. Cells were then spotted on plates, were incubated at 30 °C for two days and pictures were taken.

β-galactosidase assays

Overnight saturated cultures of *Caulobacter* cells harbouring lacZ reporter plasmids were diluted ≥50X in fresh medium and incubated at 30 °C until OD_{660} of 0.3 to 0.5. 100 µl samples were collected in a 96 well plate and kept at -80 °C until measurement.

Then, 50 µl of aliquots of the previously frozen samples were thaw and immediately treated with 50 µl Z buffer (60 mM Na_2HPO_4, 40 mM NaH_2PO_4, 10 mM KCl, 1 mM $MgSO_4$, pH 7.0) supplemented with 0.1 g polymyxin B and 0,27 % (v/v) β-mercaptoethanol for 30 min at 28 °C. To this, 150 µl of Z buffer was added, followed by 50 µl of 4 mg/ml O-nitrophenyl-β-D-galactopyranoside (ONPG). Then, ONPG hydrolysis was measured at 30 °C for 30 min. The activity of the β-galactosidase expressed in miller units (MU) was calculated using the following equation: MU = (OD_{420} × 1,000) / [OD_{660} × t × v] where "t" is the time of the reaction (min), and "v" is the volume of cultures used in the assays (ml). Experimental values were the average of three independent experiments.

Microscopy

Strains grown in PYE were imaged either in exponential or stationary phase using 1.5 % agar pads with the indicated medium. Cells in osmotic shock conditions were pelleted and washed twice with the indicated stress medium and imaged in 1.5 % agar pads maintaining the stress condition. Images were obtained using Axioskop microscope (Zeiss), Orca-Flash 4.0 camera (Hamamatsu) and Zen 2.3 software (Zeiss). Temperature (30 ºC) was maintained stable during microscopy analysis using the Tempcontrol 37-analog 1 channel equipment (HemoGenix®) coupled to the Axioskop microscope. Images were processed with ImageJ. Demographs were obtained with MicrobeJ by segmenting each cell, integrating fluorescence, sorting cells by length and plotting fluorescence intensity and cellular widths to indicate the relative position of the protein fusions, in which 0 represents mid-cell and 2 or -2 the cell poles (Ducret *et al*., 2007).

180

181 **Protein purification**

182 In order to immunize rabbits for production of ChvI polyclonal antibodies His6-ChvI
183 was purified as follows. A BL21(DE3) strain harboring plasmid pET-28a-*chvI* was
184 grown in LB medium supplemented with kanamycin until an OD_{600} of 0.7 was reached.
185 IPTG (isopropyl-β-D-thiogalactopyranoside) (Thermo Fisher Scientific) was added at
186 a final concentration of 1 mM, and the culture was incubated at 37 °C for 4 h. Then,
187 cells were harvested by centrifugation for 20 min at 5,000 *g* and 4 °C. The pellet was
188 resuspended in 20 ml BD buffer (20 mM Tris-HCl [pH 8.0], 500 mM NaCl, 10%
189 glycerol, 10 mM MgCl2, 12.5 mM imidazole) supplemented with complete EDTA-free
190 protease cocktail inhibitor (Roche), 400 mg lysozyme (Sigma), and 10 mg DNase I
191 (Roche) and incubated for 30 min on ice. Cells were then lysed by sonication and the
192 lysate by centrifugation (12,000 rpm for 30 min at 4 °C) was loaded on a Ni-
193 nitrilotriacetic acid (Ni-NTA) column and incubated for 1 h at 4 °C with end-over-end
194 shaking. The column was then washed with 5ml BD buffer, 3ml Wash1 buffer (BD
195 buffer with 25 mM imidazole), 3ml Wash2 buffer (BD buffer with 50 mM imidazole),
196 and 3ml Wash3 buffer (BD buffer with 75 mM imidazole). Proteins bound to the column
197 were eluted with 3ml elution buffer (BD buffer with 100 mM imidazole) and aliquoted
198 in 300 μl fractions. All the fractions containing the protein of interest (checked by
199 Coomassie blue staining) were pooled and dialyzed in dialysis buffer (50 mM Tris [pH
200 7.4], 12.5 mM MgCl2).

201

202 **Immunoblot analysis**

Proteins crude extracts were prepared by harvesting cells from exponential growth phase (OD_{660} ~0.3). The pellets were then resuspended in SDS-PAGE loading buffer by normalizing to the OD_{660} before lysing cells by incubating them for 10 min at 95 °C. The equivalent of 0.5 ml of cult (OD_{660} = 0.3) was loaded and proteins were subjected to electrophoresis in a 12% SDS-polyacrylamide gel, transferred onto a nitrocellulose membrane then blocked overnight in 5% (wt/vol) nonfat dry milk in phosphate buffer saline (PBS) with 0.05% Tween 20. Membrane was immunoblotted for ≥ 3 h with primary monoclonal anti-GFP (1:5,000) antibodies (JL8, Clontech-Takara), then followed by immunoblotting for ≤ 1 h with secondary antibodies: 1:5,000 anti-mouse linked to peroxidase (Dako Agilent), and vizualized thanks to Clarity™ Western ECL substrate chemiluminescence reagent (BioRad) and Amersham Imager 600 (GE Healthcare).

Chromatin immunoprecipitation followed by deep sequencing (ChIP-Seq) assay.

A ChIP-Seq protocol was followed as described by Coppine *et al.* (2020). Briefly, 80 ml of mid-log-phase cells (OD_{660} of 0.6) were cross-linked in 1% formaldehyde and 10 mM sodium phosphate (pH 7.6) at room temperature (RT) for 10 min and then for 30 min on ice. Cross-linking was stopped by addition of 125 mM glycine and incubated for 5 min on ice. Cells were washed twice in phosphate buffer solution (PBS; 137 mM NaCl, 2.7 mM KCl, 10 mM Na_2HPO_4, 1.8 mM KH_2PO_4, pH 7.4) resuspended in 450 μl TES buffer (10 mM Tris-HCl [pH 7.5], 1mM EDTA, and 100 mM NaCl), and lysed with 2 μl of Ready-lyse lysozyme solution for 5 min at RT. Protease inhibitors (Roche) were added, and the mixture was incubated for 10 min. Then, 550 μl of ChIP buffer (1.1%

227 Triton X-100, 1.2 mM EDTA, 16.7 mM Tris-HCl [pH 8.1], and 167 mM NaCl, plus
228 protease inhibitors) was added to the lysate and incubated at 37 °C for 10 min before
229 sonication (2 x 8 bursts of 30 sec on ice using a Diagenode Bioruptor) to shear DNA
230 fragments to a length of 300 to 500 bp. Lysate was cleared by centrifugation for 10
231 min at 12,500 rpm at 4 °C, and protein content was assessed by measuring the OD_{280}.
232 Then, 7.5 mg of proteins was diluted in ChIP buffer supplemented with 0.01% SDS
233 and precleared for 1 h at 4 °C with 50 μl of SureBeads Protein A Magnetic Beads
234 (BioRad) and 100 μg bovine serum albumin (BSA). One microliter of polyclonal anti-
235 ChvI antibodies was added to the supernatant before overnight incubation at 4 °C
236 under gentle agitation. Next, 80 μl of BSA presaturated protein A-agarose beads was
237 added to the solution and incubated for 2 h at 4 °C with rotation, washed once with
238 low-salt buffer (0.1% SDS, 1% Triton X-100, 2mM EDTA, 20 mM Tris-HCl [pH 8.1],
239 150 mM NaCl), once with high-salt buffer (0.1% SDS, 1% Triton X-100, 2mM EDTA,
240 20 mM Tris-HCl [pH 8.1], 500 mM NaCl), once with LiCl buffer (0.25 M LiCl, 1% NP-
241 40, 1% deoxycholate, 1mM EDTA, 10 mM Tris-HCl [pH 8.1]), and once with TE buffer
242 (10 mM Tris-HCl [pH 8.1] 1mM EDTA) at 4 °C, followed by and a second wash with
243 TE buffer at RT. The DNA-protein complexes were eluted twice in 250 μl freshly
244 prepared elution buffer (0.1 M NaHCO3, 1% SDS). NaCl was added at a concentration
245 of 300 mM to the combined eluates (500 μl) before overnight incubation at 65 °C to
246 reverse the cross-link. The samples were treated with 20 μg of proteinase K in 40mM
247 EDTA and 40 mM Tris-HCl (pH 6.5) for 2 h at 45 °C. DNA was extracted using a
248 Nucleospin PCR cleanup kit (Macherey-Nagel) and resuspended in 50 μl elution buffer
249 (5 mM Tris-HCl [pH 8.5]). DNA sequencing was performed using an Illumina HiSeq

4000 instrument (Bio.be). NGS data were analysed as described in Coppine et al., 2020.

RNA-seq.

WT and Δ*chvI* cells were grown O.N to OD_{660} 0.3 and, then, exposed to 6% sucrose for 4 h. Thereafter, total RNA was extracted with RNeasy® Protect Bacteria Kit from Qiagen and following manufacturers instructions. The quantity and quality (A260/A280 ration) of RNA was determined with a Thermo Scientific ™ Nanodrop ™ One Microvolume UV-Vis Spectrophotometer. Samples were sent for analysis at Bio.BE company and analysed using Galaxy (Afgan *et al.,* 2018).

***In vivo* ^{32}P labelling**

Cells were grown overnight in PYE, then washed twice and grown in M5G medium lacking phosphate and was grown overnight in M5G with 0.05 mM phosphate to OD_{660} of 0.3. Then, one milliliter of culture was labelled for 4 min at 30 °C using 30 μCi γ-[^{32}P]ATP (PerkinElmer). For osmotic shock experiments, samples were incubated with 6% sucrose for 7 minutes at 30 °C. Then, cells were pelleted for 2 minutes at 15000 rpm and the supernatant removed completely without disturbing the pellets. Cell pellets were resuspended in 50 μl Lysis Buffer (50mM Tris pH 7.0, 150mM NaCl, 80 mM EDTA, 2% Triton X100; sterilised with 2 μm Acrodisc syringe filters) by pipetting. Lysed samples were incubated 3 minutes on ice. And 450 μl of cold LBS was added and proteins were collected using centrifugation for 15 minutes at 13000 and 4 °C. Then, 40 μl of SureBeads Protein A Magnetic Beads (BioRad) were washed 4 times in 1 ml PBS + 0.1% Tween (PBS-T) and finally resuspended in 65 μl. Thereafter, 3 μl

of anti-ChvI antibody were added to the washed protein A-agarose beads and incubated at RT in a shaker at 1300 rpm. Protein A beads with anti-ChvI antibodies were washed 3 times with PBS-T and 1 time with cold (4 ºC) Low Salt Buffer (LSB; 50mM Tris pH 7.0, 100mM NaCl, 50 mM EDTA, 2% Triton X100; sterilised with 2 μm Acrodisc syringe filters), immediately resuspended in 50 μl LSB and kept in ice. ChvI immunoprecipitation (IP) was performed by adding the Protein A beads with anti-ChvI antibodies previously prepared to the cell-free protein samples, and incubating at 4 ºC with rotation for 90 minutes. IP samples were washed 1 time in 1ml LSB and 3 times in 1 ml High Salt Buffer (50mM Tris pH 7.0, 500mM NaCl, 50 mM EDTA, 0.1% Triton X100; sterilised with 2 μm Acrodisc syringe filters). Samples were eluted using 25 μl of 2,5X SDS-loading Buffer and incubation at 37 ºC for 5 minutes. Samples with SDS loading Buffer were separated from magnetic beads, and 20 μl loaded on a SDS-Page gel and run at 200V-50mA-100W. The gel was dried for 1h at 70 ºC under vacuum in a Model 583 Gel Dryer (BioRad). Finally, the dried gel was exposed on phosphoscreen for 5 days and revealed using a Cyclone Plus Phosphor Imager (PerkinElmer).

Results

High osmolyte concentration in M2G impairs growth of *chvIG* mutants

It was shown previously that *C. crescentus chvIG* mutants failed to grow in minimal media with xylose as sole carbon source (M2X), while these mutants grew similarly to WT cells in complex media (PYE) (Stein *et al.,* 2021). Likewise, we observed that mutants inoculated in M2G (with glucose as sole carbon source) in both solid and liquid media were impaired for growth (Fig. 1A-B). To date, the cause for growth impairment in *chvIG* mutants in minimal media has not been determined. Considering that stressful conditions are present in synthetic minimal media (M2G or M2X) but missing in PYE, we tested osmolytes as causative agents. Indeed, the synthetic minimal media M2G contains a higher concentration of osmolytes than the complex media PYE (Hocking *et al.,* 2012). Therefore, we assessed the viability of *chvIG* mutants on plates lacking Na^+ and K^+ salts (Fig. 1A; M2G 0% Na^+, K^+). In these conditions the *chvI* mutant grew similarly to WT cells. We also reduced these osmolytes in liquid cultures, and observed that growth was restored in the *chvI* mutant when half (and below) of the regular concentration found in M2G was used (Fig. 1B; M2G 50% Na^+, K^+). Furthermore, we observed that adding osmolytes (NaCl or sucrose) to complex media impaired growth and decreased viability of a *chvI* mutant (Fig. 1A; PYEX + 40 mM NaCl; PYE + 6% Sucrose). Additionally, ectopic expression of *chvI* from the xylose-inducible promoter (P_{xylX}*::chvI*) in a *chvI* mutant restored growth in PYEX plates supplemented with NaCl whereas expressing back *chvI* in a *chvIG* mutant did not (Fig. 1A). Finally, while a phospho-mimetic mutant of *chvI* (*chvI*$_{D52E}$) grew similarly to WT, a phospho-ablative mutant of *chvI* (*chvI*$_{D52A}$) failed to propagate

in M2G (Fig. 1C). Together, our data show that a fully functional ChvIG TCS is required to survive and grow in hyperosmotic environments.

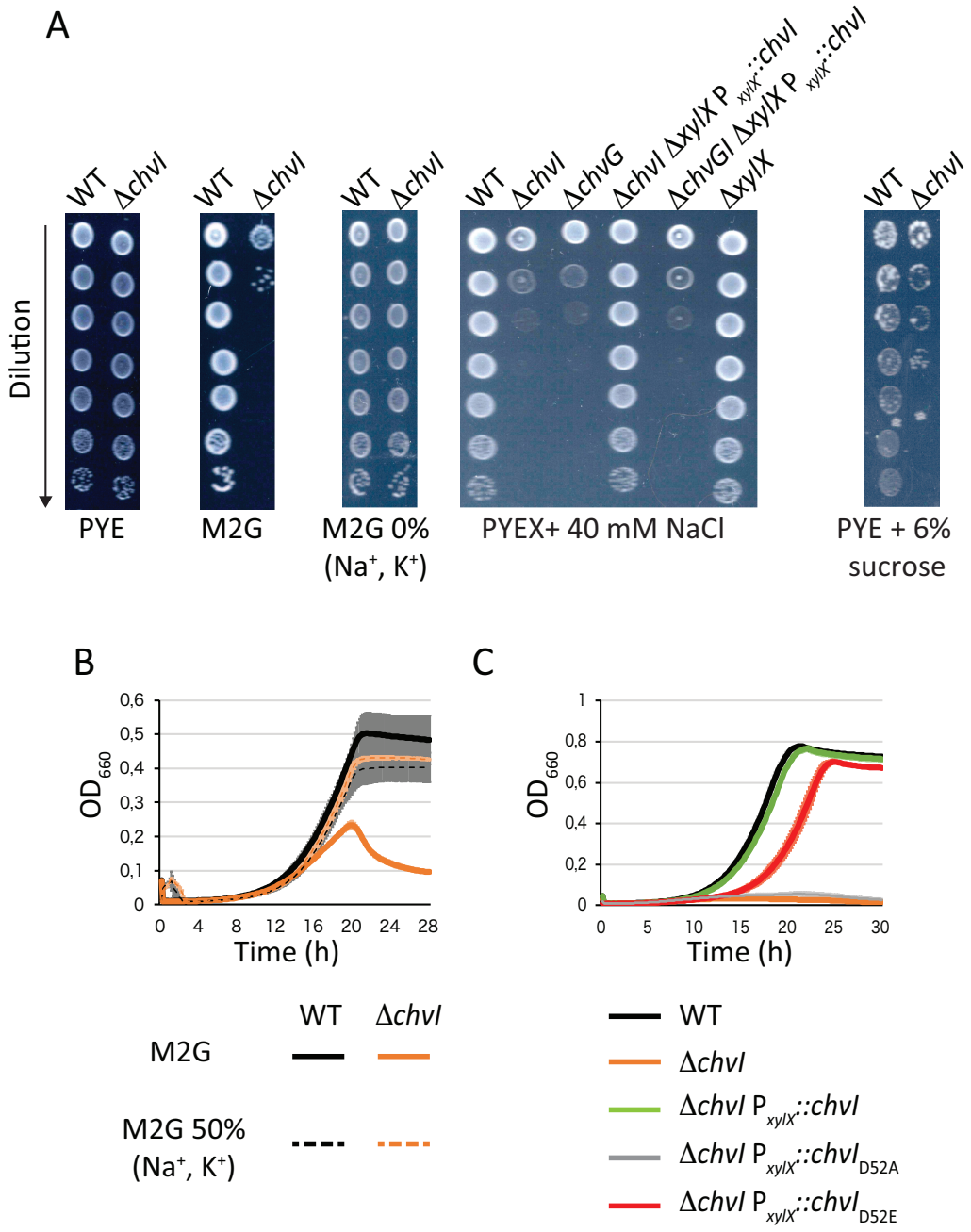

Fig. 1. Viability and growth of *chvGI* mutants upon hyperosmotic conditions. (A) Viability of WT and Δ*chvI* cells in complex (PYE) and synthetic minimal media (M2G) plates with varying osmolytes concentrations. For complementation assays, PYE was supplemented with 0.1% xylose (PYEX). (B) Growth in minimal media with 100% (solid lines) or 50% (dashed lines) Na_2HPO_4 and KH_2PO_4 concentrations referred to M2G. (C) Growth in M2G of mutants complemented with *chvI* copies from either WT, phospho-ablative ($chvI_{D52A}$) or phospho-mimetic ($chvI_{D52E}$) mutants. Data in (B) and (C) represent the average value of biological replicates (n=3, error bars show standard deviation).

Mutations in *chvT* and *ntrX* improve fitness of the *chvI* mutant under osmotic stress

Considering that mutations in *chvT* and *ntrX* partially alleviated the growth impairment of *chvI* mutants in minimal media (Stein *et al.*, 2021), we tested whether *chvT* or *ntrX* inactivation could also partially protect *chvI* mutants from hypertonic conditions. We first confirmed that a Δ*chvI* mutant was impaired for growth under osmotic stress by using an excess of KCl in PYE (Fig. 2A). In contrast, neither *ntrX* nor *chvT* inactivation did interfere with growth in PYE + KCl conditions compared to WT (Fig. 2A). Interestingly, we observed that inactivating *ntrX* in a Δ*chvI* background restored growth similar to WT, while the Δ*chvT* mutation led to cultures with slightly higher OD in liquid cultures. Thus, these data suggest that growth impairment in liquid upon osmotic upshift in a *chvI* mutant is primarily caused by upregulation of ChvT or NtrX.

As expected, Δ*chvI* cells poorly grew on PYE plates supplemented with KCl whereas the growth of Δ*chvT* cells was similar to the WT on the same plates (Fig. 2B). Surprisingly, in contrast to liquid cultures (Fig. 2A), we observed that Δ*ntrX* cells did not grow as the WT in PYE plates but this growth delay was not aggravated in the presence of KCl excess (Fig. 2B). Nevertheless, inactivating either *ntrX* or *chvT* in a Δ*chvI* background partially restored growth on KCl plates (Fig. 2B). These data indicate that additional cell envelope defects in *chvI* mutants are responsible for growth impairment on hypertonic plates. Altogether, these data suggest that the homeostasis of the cell envelope is lost in *chvIG* mutants, leading to a hypersensitivity to osmolytes.

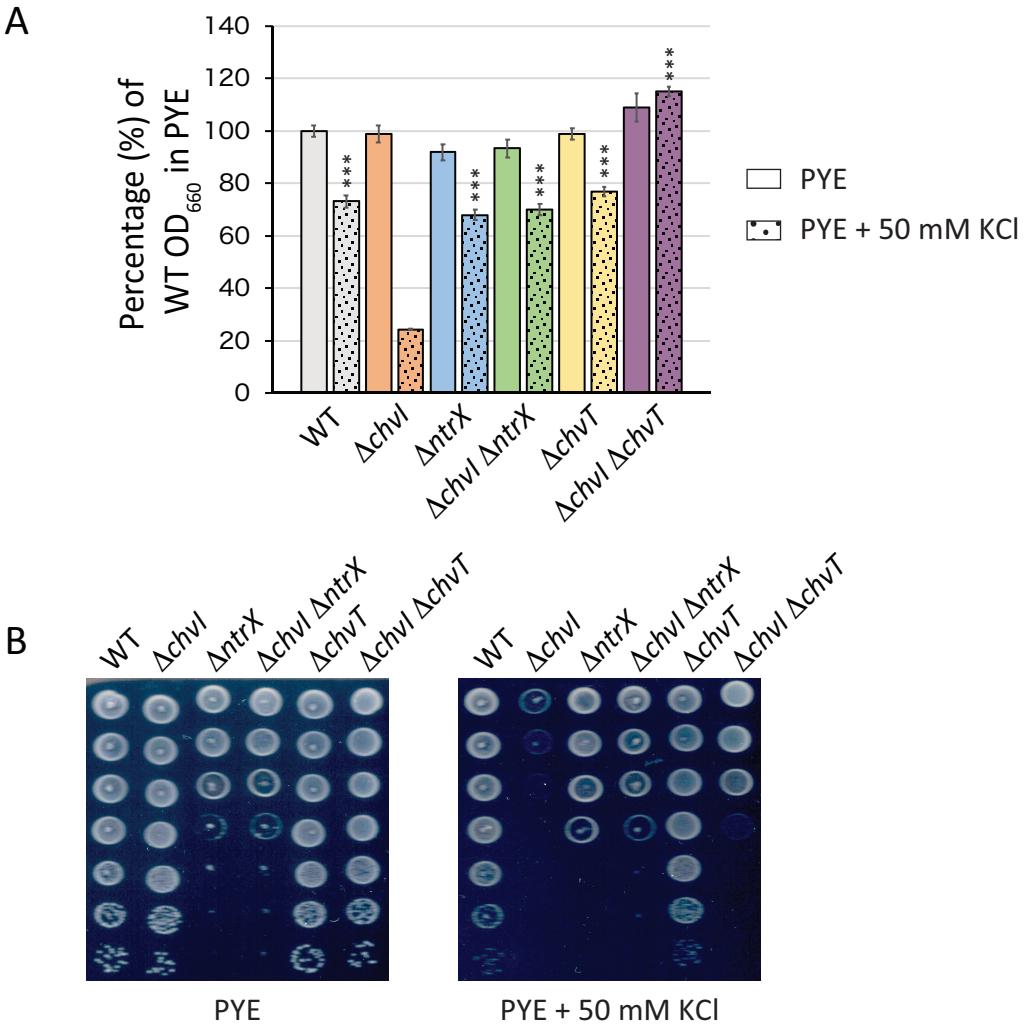

Fig. 2. Growth and viability of *chvI*, *chvT* and *ntrX* mutants in hypertonic conditions. (A) Percentage of optical density (OD_{660}) after 22 hrs of growth in PYE liquid with (dotted bars) or without 50 mM KCl (solid bars). The data represent the average values of biological replicates (n=3, error bars show standard deviation). *** = $p < 0.0001$, single factor ANOVA analysis of OD_{660} after 22 hrs of growth in PYE supplemented with 50 mM KCl compared Δ*chvI* cells. (B) Viability of single (Δ*chvI*, Δ*chvT* and Δ*ntrX*) and double (Δ*chvI* Δ*chvT* and Δ*chvI* Δ*ntrX*) mutants on PYE agar with or without 50 mM KCl.

ChvI regulon reveals osmotic stress and cell envelope-related target genes

Transcriptomic analyses were previously performed on a Δ*chvI* mutant overexpressing the phospho-mimetic mutant $chvI_{D52E}$ in PYE (Stein *et al.*, 2021). Nonetheless, cells expressing $chvI_{D52E}$ as the only copy, either from its own promoter at the endogenous *chvI* locus (P_{chvI}::$chvI_{D52E}$) or ectopically from the xylose-inducible promoter (P_{xylX}::$chvI_{D52E}$) led to a slight growth delay and cell filamentation (Fig. 1C and Fig. S1).

356 This suggests either that ChvI$_{D52E}$ does not perfectly mimic phosphorylated ChvI or
357 that unphosphorylated ChvI is also required for optimal growth in synthetic minimal
358 media. Hence, we determined the ChvI regulon of WT cells grown in M2G by using
359 ChIP-seq with polyclonal antibodies targeting ChvI, which allowed to unveil the DNA
360 regions directly bound by ChvI (Fig. 3A, Supplementary table 4).
361 From our experiment, 169 DNA binding sites were identified for ChvI (Fig. 3A, Table
362 S4). About 30% of them (52) correspond to sequences in the vicinity of 101 genes
363 previously identified in the regulon of ChvI$_{D52E}$ in PYE. The 117 remaining peaks
364 correspond to promoter regions of potentially new candidates. Interestingly, the top
365 target is the promoter region of *chvT* itself, suggesting that ChvI regulates ChvT both
366 (i) directly at the transcriptional level and (ii) indirectly at the post-transcriptional level
367 via transcriptional activation of the sRNA *chvR* (Fig. 3A). Beside *chvT* and *chvR*, we
368 identified potential new targeted genes involved in (i) cell division, morphology and
369 peptidoglycan (PG) synthesis, such as *mreB*, *ftsZ*, *ftsN* and *dipM*; and (ii) general
370 stress response (GSR), such as *sigT* (sigma factor T), *nepR* (*sigT* antagonist) and
371 *phyKR* (TCS regulating NepR activity negatively).
372 By performing RNA-seq on WT and Δ*chvI* cells grown in PYE and incubated a few
373 hours in PYE supplemented with 6% sucrose, we found 169 genes with ≥1.5-fold
374 change (Supplementary Table 4). From these binding sites, ~69% correspond to
375 genes identified in our ChIP-seq experiment and ~31% to genes identified in the
376 previous regulon generated by Stein *et al.* (2021) (Table S4). To further confirm some
377 of the new targeted genes, we tested their expression by measuring their promoter
378 activity upon osmotic shock. As shown in Fig 3B, the activity of *dipM* and *ftsN*
379 promoters was significantly lower in the *chvI* mutant compared to WT, while *phyR*

promoter activity was significantly higher in Δ*chvI* than in WT. In contrast, the *nepR* promoter had similar activity in both WT and Δ*chvI* strains. These results suggest that ChvI can work as an activator (e.g. *dipM* and *ftsN*) or a repressor (e.g. *phyR*) of gene expression.

Interestingly, *hprK* is part of the SigT regulon determined upon osmotic shock (Tien *et al.*, 2018). Given that *hprK* is part of the same operon as *chvIG*, we tested whether the entire operon *chvIG-hprK* could be under the control of SigT. Consistently, we found that the *chvI* promoter (P_{chvI}) was significantly higher in the Δ*sigT* mutant compared to WT whereas the activity of P_{chvI} was strongly reduced in the Δ*chvI* mutant (Fig. S2A). Thus, SigT is a negative regulator of ChvI while ChvI is subjected to a positive feedback loop. Considering that *phyR* promoter activity was higher in a Δ*chvI* background (Fig. 3C), this indicates that ChvI regulates negatively SigT by inhibiting PhyR. Together, these data suggest that both SigT and ChvI antagonise each other. Overall, our data show that ChvI controls the expression of genes involved in cell envelope homeostasis, in response to osmotic stress.

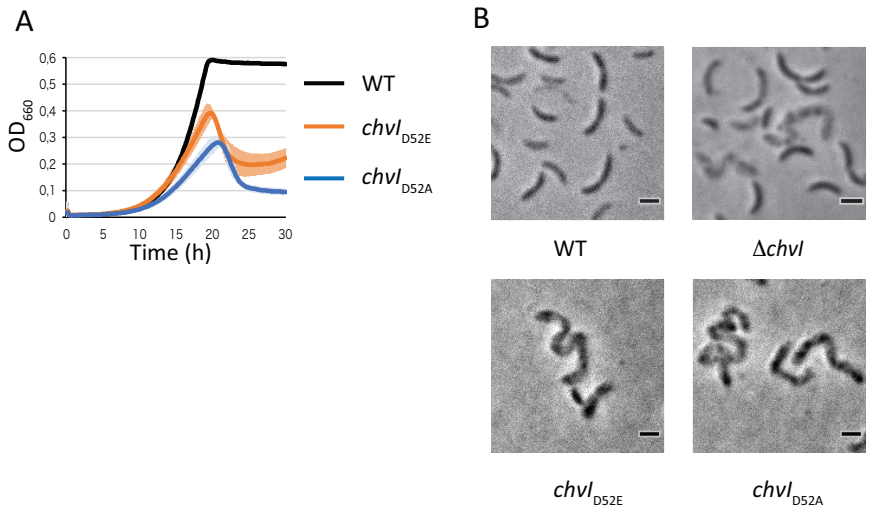

Figure S1. Growth and morphology of *chvI* mutant strains in synthetic minimal media. (A) Growth of WT, $chvI_{D52E}$ and $chvI_{D52A}$ mutant strains in M2G. The data represent the average values of biological replicates (n=3, error bars show standard deviation). (B) Morphology of WT, Δ*chvI*, $chvI_{D52E}$ and $chvI_{D52A}$ cells after 48 hrs of incubation in M2G. Scale bars in microscopy images correspond to 1 μm.

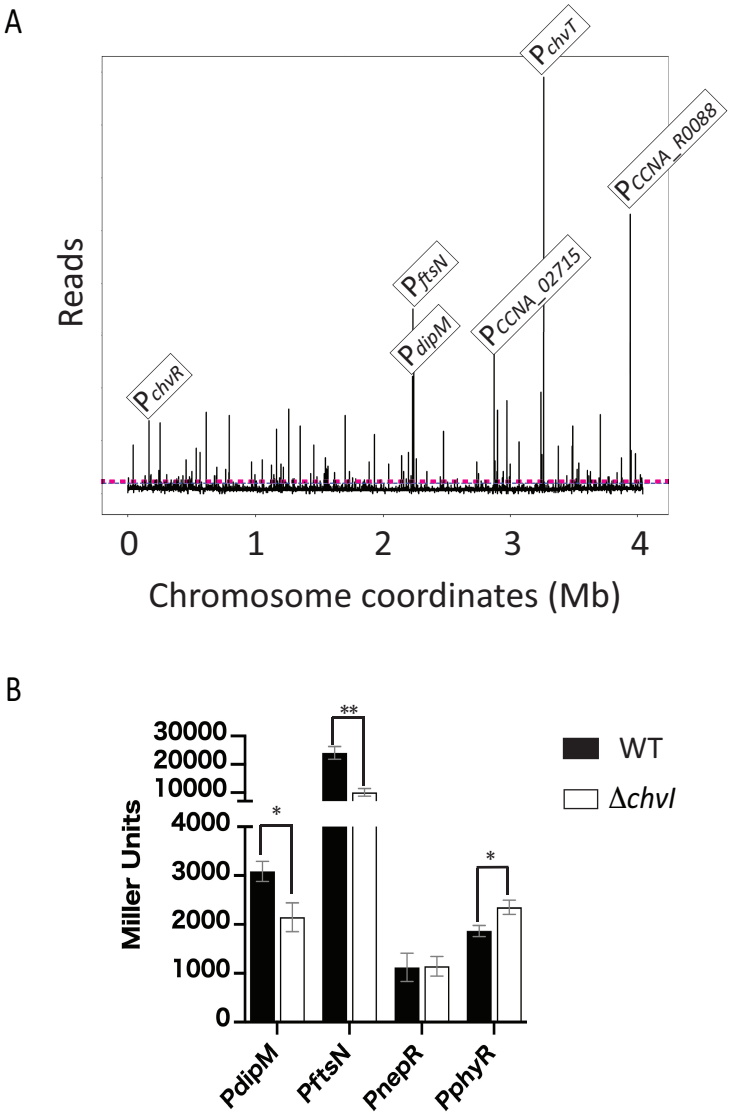

Fig. 3. ChvI target genes determined by ChIP-seq and validated by β-galactosidase assays. (A) Genome-wide occupancy of ChvI on the chromosome of *C. crescentus* determined by ChIP-seq on WT strain grown in M2G. The x-axis represents the corrdinates on the genome (Mb), the y-axis shows the normalized ChIP-Seq read abundance in reads. Some top hits, corresponding to the promoter regions of *chvT*, *CCNA_R0088*, *ftsN, CCNA_02715*, *chvR* and *dipM* operon, are highlighted. (B) Activity of the *dipM*, *ftsN*, *nepR* and *phyR* promoters (Miller Units) in WT (black bars) and Δ*chvI* (white bars) cells grown in PYE. The data represent the average values of biological replicates (n=3, error bars show standard deviation). * = $p < 0.05$, ** = $p < 0.01$, single factor ANOVA analysis of β-galactosidase activity.

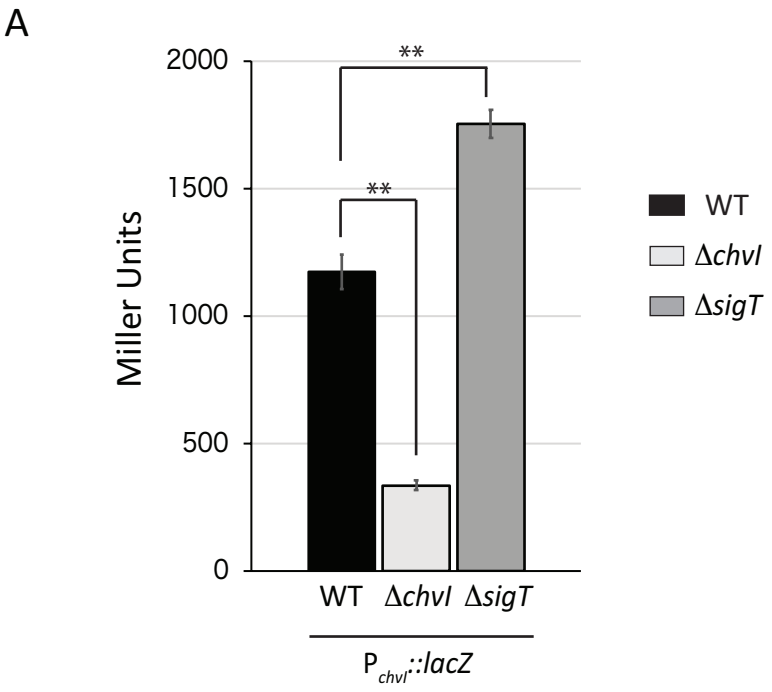

Figure S2. Activity of the *chvI* promoter is regulated by the sigma factor T. (A) Activity of the *chvI* promoter (Miller Units) in WT (black bars), Δ*chvI* (light grey bars) Δ*sigT* (dark grey bars) grown in PYE. The data represent the average values of biological replicates (n=3, error bars show standard deviation). ** = $p < 0.01$ Single factor ANOVA analysis of β-galactosidase activity.

ChvI is phosphorylated under osmotic upshift

Since both single Δ*chvG* and Δ*chvI* mutants are sensitive to osmotic upshift (Fig 1A), this suggests that ChvI might be phosphorylated and activated by ChvG in such stressful conditions. We tested this hypothesis by determining the *in vivo* phosphorylated levels of ChvI (ChvI~P) with or without osmotic shock. In order to facilitate uptake of [γ-^{32}P] ATP, *Caulobacter* cells are grown in a medium depleted for the phosphate salts Na_2HPO_4 and KH_2HPO_4 (M5GG). Hence, K^+ and Na^+ concentrations in M5GG are respectively 1.01 mM and 1.02 mM, which is much less that in M2G (7.75 mM of K^+ and 12.25 mM of Na^+). At such low concentrations of osmolytes, the Δ*chvI* strain grew, as expected, similarly to WT in M5GG (Fig. 4A). In contrast and in agreement with our previous findings, the growth of the Δ*chvI* mutant

was severely impaired in M5GG supplemented with 6% sucrose compared to WT (Fig. 4A). Consistent with these data, we observed that ChvI was barely phosphorylated in WT grown in M5GG while no ChvI~P was detected in Δ*chvG* (Fig. 4B). More importantly, ChvI was hyperphosphorylated in cells grown under osmotic shock with sucrose (Fig. 4C-D).

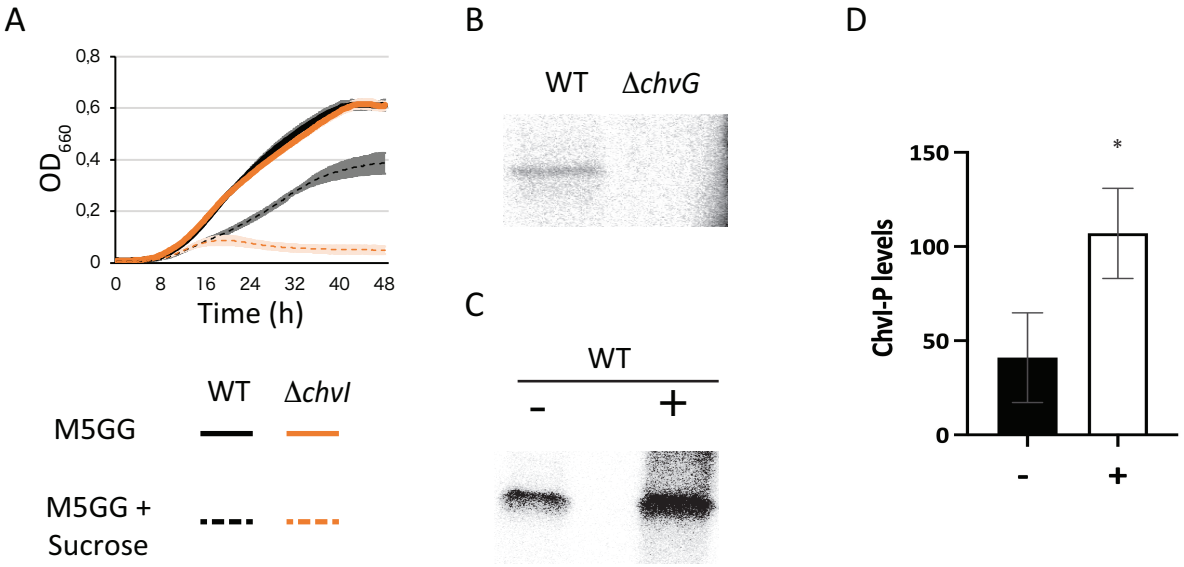

Fig. 4. ChvG-dependent phosphorylation of ChvI is stimulated upon osmotic shock. (A) Growth of WT (black) and Δ*chvI* mutant (orange) in M5GG with (dashed lines) or without (solid lines) 6% sucrose. The data represent the average value of biological replicates (n=3, error bars show standard deviation). (B) *in vivo* phosphorylation levels of ChvI in WT and Δ*chv*G mutant grown in M5GG. (C) *in vivo* phosphorylation levels of ChvI in WT grown in M5GG without (-) or with (+) 6% sucrose. (D) Quantified *in vivo* phosphorylation levels of ChvI in the same growth conditions than in (C). The data represent the average values of biological replicates (n=3, error bars show standard deviation). * = $p < 0.05$, single factor ANOVA analysis of ChvI phosphorylation.

ChvGI is sensitive to peptidoglycan synthesis inhibition

Stress response systems surveying cell envelope homeostasis in Gram-negative bacteria are sensitive to different stressful conditions including osmotic shock (Humphreys *et al.,* 1999; Jubelin *et al.,* 2005; Laubacher & Ades. 2008; Cho *et al.,* 2014). Therefore, we first tested growth and viability in other cell envelope stressors,

438 such as acidic pH, detergent and antibiotics targeting the outer membrane or the PG
439 synthesis machinery. We did not observe significant impacts on fitness between WT
440 and Δ*chvI* cells under treatment with acidic stress (Fig. 5A), A22 drug targeting the
441 actin-like protein MreB (Fig. 5B, D), SDS and polymyxin B detergents (Fig. S3A-B). In
442 contrast, exposure to mecillinam, which inhibits the the penicillin binding protein 2
443 (PBP2) transpeptidase activity thereby obstructing PG crosslinking during elongation,
444 significantly impaired growth of Δ*chvI* compared to WT (Fig. 5C-D). Considering that
445 a *chvI* mutant was also sensitive to vancomycin (Vallet *et al.,* 2018), which targets the
446 D-Ala-D-Ala moiety of the PG precursors thereby inhibiting PG crosslinking, we
447 assessed the impact of both vancomycin and mecillinam on the *chvI* promoter activity
448 in synthetic media M5GG (Fig. 5.E). We observed that growth was severely affected
449 in the Δ*chvI* mutant after six hours of growth with mecillinam and to a lesser extent
450 with vancomycin. In comparison to untreated cells, the activity of the P_{chvI}*::lacZ*
451 transcriptional reporter significantly increased after six hours of exposure to mecillinam
452 while vancomycin treatment did not influence *chvI* expression. Interestingly, although
453 the activity of P_{chvI}*::lacZ* decreased in Δ*chvI* cells treated with mecillinam, it remained
454 significantly higher than in the untreated Δ*chvI* cells. These data suggest that upon
455 mecillinam treatment, the expression of the *chvIG-hprK* operon is induced not only by
456 ChvI itself but also in a ChvI-independent way.
457
458

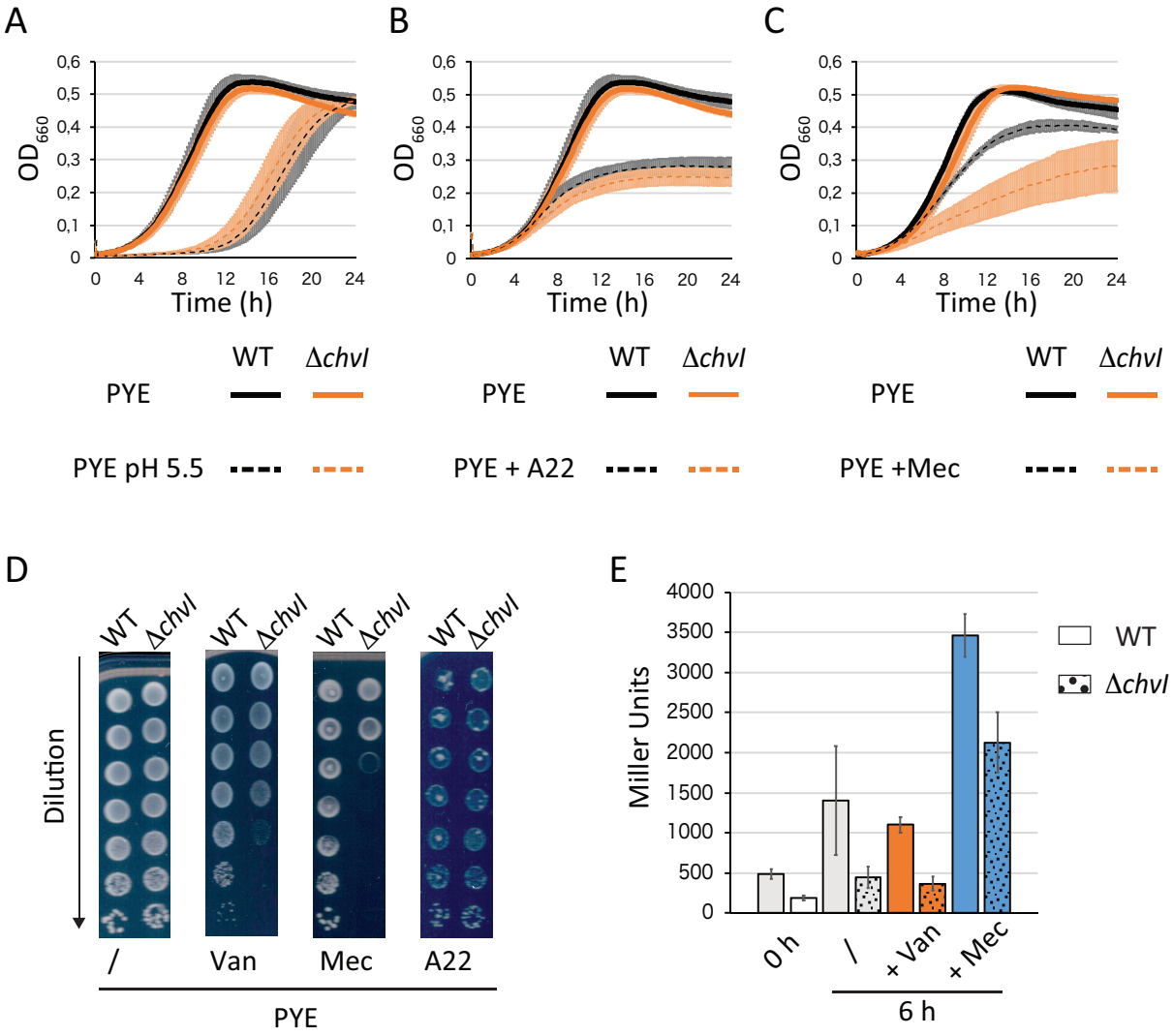

459

460

461

462

463

464

465

Fig. 5. ChvI expression is activated upon mecillinam treatment (A-C) Growth of WT and Δ*chvI* mutant cells in PYE at acidic pH 5.5 (A) or supplemented with either A22 (B) or mecillinam (C). (D) Viability of WT and Δ*chvI* mutant upon treatment with mecillinam (Mec) and A22. (E) Activity of the *chvI* promoter (Miller Units) in WT (solid bars) and Δ*chvI* (dashed bars) cells grown in minimal media M5GG treated for 6 hrs with vancomycin (Van) or mecillinam (Mec). The data in figures (A-C) and (E) represent the average values of biological replicates (n=3, error bars show standard deviation). The drugs were used at the following concentrations: A22 (2.5 μg ml^{-1}), vancomycin (10 μg ml^{-1}) and mecillinam (100 μg ml^{-1}).

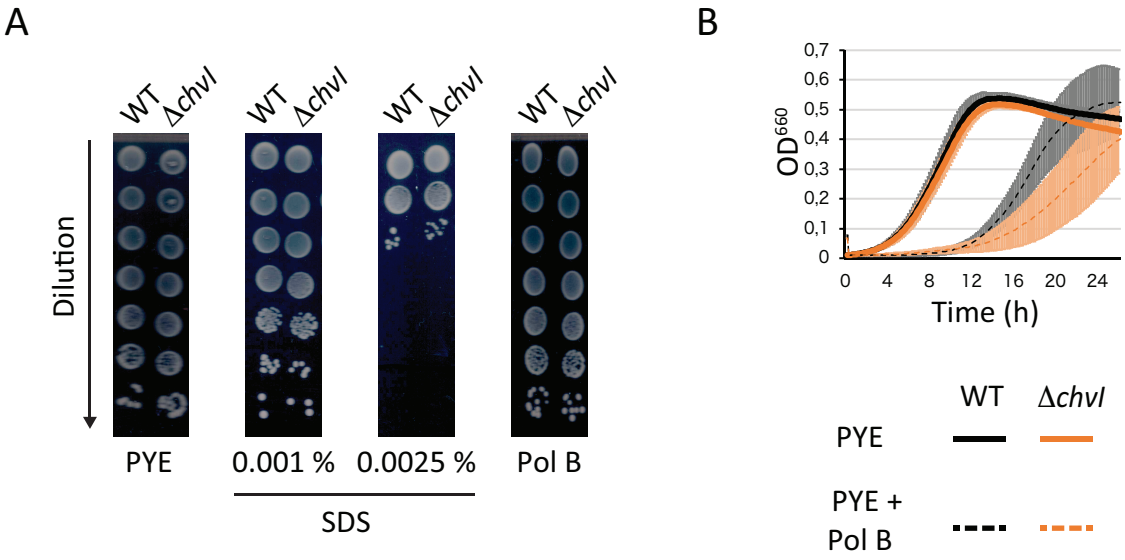

Figure S3. Δ*chvI* is not sensitive to SDS and polymixin B treatment. (A) Viability of Δ*chvI* cells on plates supplemented with 0.001 % or 0.0025% sodium dodecyl sulfate (SDS), 10 μg ml^{-1} polymixin B (Pol B). (B) Growth of WT (black) and Δ*chvI* (orange) cells in PYE with (dashed lines) or without (solid lines) 5 μg ml^{-1} polymixin B (Pol B).

ChvG relocates from patchy-spotty to midcell upon osmotic shock

Intriguingly, the HK ChvG was previously found in an automated large scale analysis for protein localisation as displaying a patchy-spotty distribution typically observed with PG-related proteins (Werner *et al.,* 2009). Therefore, we constructed fluorescent protein fusions to analyse ChvG and ChvI localisation patterns on PYE and M2G pads. First, we confirmed that GFP fusions to the N- or C-terminal extremity of ChvG or ChvI were stable and functional, as attested by western blot analyses and growth assays (Fig. S4AB). Then, fluorescent microscopy images showed that both ChvG N- and C-terminal fusions to GFP displayed patchy-spotty localisation patterns in cells grown in PYE or M2G cultures (Fig. 6A, Fig. S4C). We also confirmed the patchy-spotty localisation pattern for the ChvG C-terminal fusion to GFP in high resolution confocal

483 microscopy (Fig. S4D). Surprisingly, when cells grown in PYE were washed in M2G
484 and imaged on M2G agar pads, we observed some cells formed foci at mid-cell (Fig.
485 6A). In contrast, cells grown in M2G, washed with PYE and imaged on PYE pad kept
486 their patchy-spotty localisation pattern (Fig. 6A). This relocation is reminiscent to what
487 was described for the PG-related proteins RodA, PBP2 and PBP1A, whose
488 localization changed from a typical patchy-spotty distribution to mid-cell when cells
489 were shifted from PYE to M2G agarose pads (Hocking *et al.,* 2012).
490 In contrast to ChvG, none of the ChvI fusions to GFP (ChvI-GFP and GFP-ChvI)
491 displayed patchy-spotty localization. Instead, the signal was diffused all over the cell
492 body, indicating that the protein remains diffuse in the cytoplasm. Neither, we could
493 observe foci formation in these mutants after transition from PYE to M2G pads (Fig.
494 6B and data not shown). Then, we wanted to assess if the catalytic activity had any
495 impact on the protein localisation. For that, we fused GFP to a full-length catalytic
496 mutant of ChvG to ($ChvG_{H309N}$), which like Δ*chvG* was unable to grow on M2G (Fig.
497 S4E-D). We observed that, similar to the WT ChvG-GFP, the $ChvG_{H309N}$-GFP showed
498 a patchy-spotty pattern when cells were grown in PYE and relocated at mid-cell when
499 shifted from PYE to M2G (Fig. 6C). However, we noticed that the fluorescent foci were
500 more conspicuous in populations of cells expressing $ChvG_{H309N}$-GFP fusions than the
501 ones expressing ChvG-GFP. Thus, our data suggest that ChvG co-localizes with PG
502 synthesis machinery independently of its kinase activity.

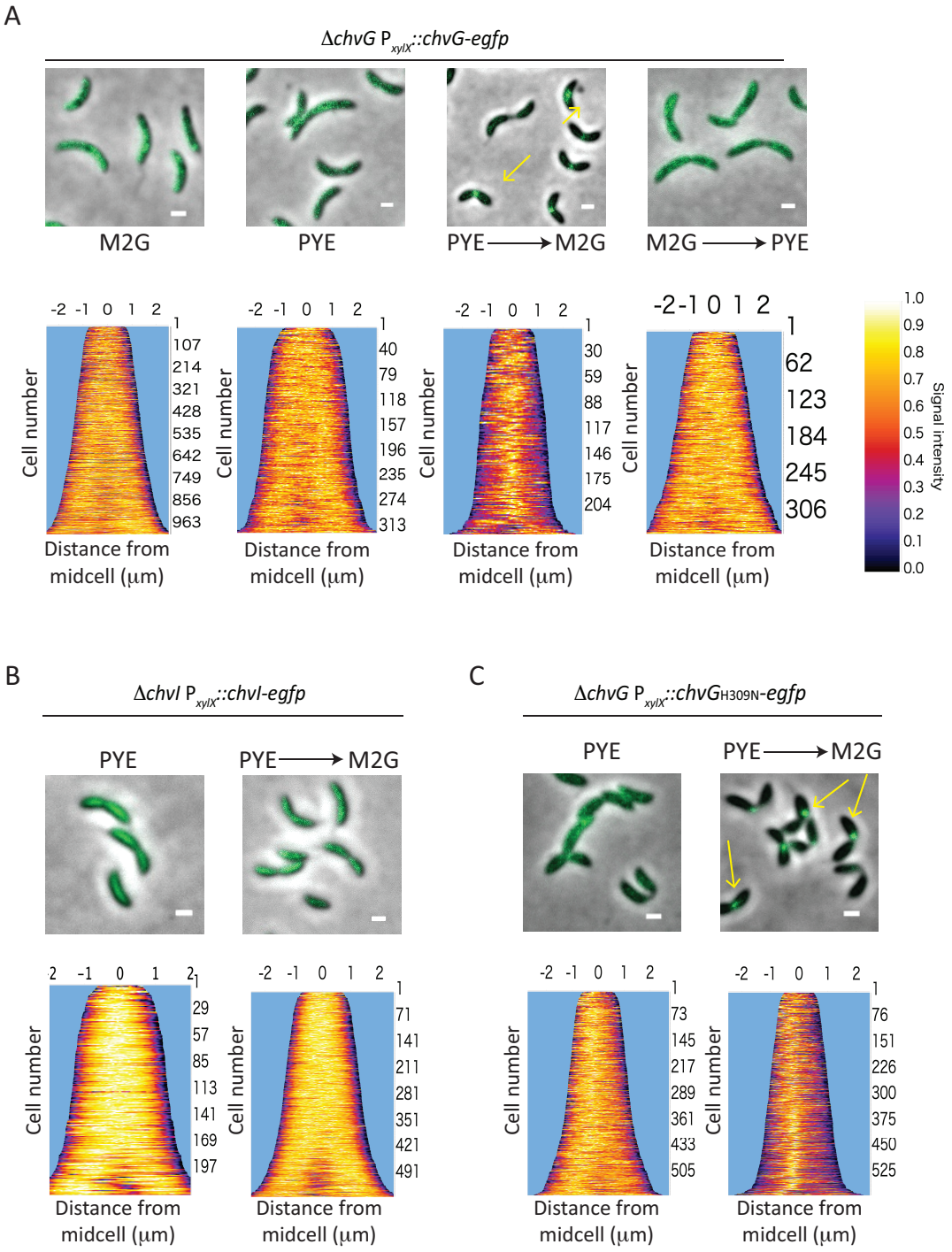

Fig. 6. ChvG relocates from a patchy-spotty pattern to mid-cell upon osmotic upshift. (A) Localisation of ChvG-eGFP in cells grown in either M2G or PYE and imaged on M2G or PYE agar pads, respectively; or cells grown in PYE, washed in M2G and imaged on M2G agarose pads (PYE → M2G); or cells grown in M2G, washed in PYE and imaged on PYE agarose pads (M2G → PYE). (B) Localisation of ChvI-eGFP in a Δ*chvI* background and (C) $ChvG_{H309N}$-eGFPin a Δ*chvG* background grown overnight in PYE and imaged on PYE agarose pads or grown in PYE, washed in M2G and imaged on M2G agarose pads (PYE → M2G). Liquid cultures and pads were supplemented with 0.1 % xylose to allow expression of ChvG, ChvI and $ChvG_{H309N}$ fused to eGFP fusions. Scale bar= 1 μm.

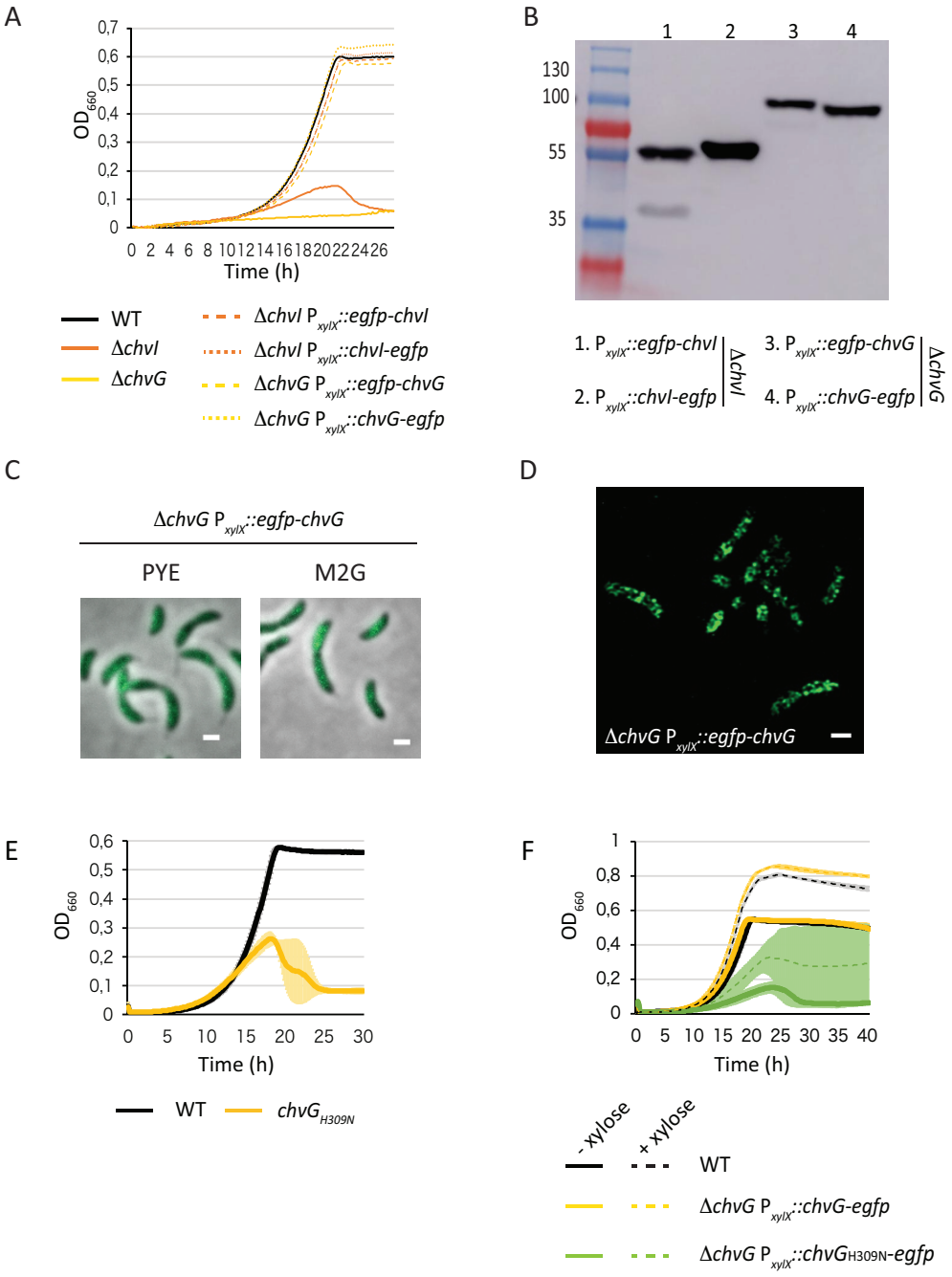

Figure S4. ChvG relocates from a patchy-spotty pattern to mid-cell upon osmotic upshift. (A) Growth of Δ*chvI* and Δ*chvG* mutants complemented with *chvI* and *chvG* N- and C-terminal eGFP fusions. (B) Immunodetection of eGFP fusions with GFP antibodies. The expected molecular weights for eGFP, eGFP-ChvI, ChvI-eGFP, eGFP-ChvG and ChvG-eGFP are 26.94, 54.33, 55.75, 85.88, 86.06 KDa, respectively. (C) Localisation of eGFP-ChvG in a Δ*chvG* background grown overnight in PYE and M2G and imaged in PYE and M2G agarose pads, respectively. (D) Confocal microscopy images of Δ*chvG* cells expressing eGFP-ChvG cells grown in PYE. (E-F) Growth upon endogenous (E) and ectopic expression (F) of $chvG_{H309N}$ in M2G. The data represent the average value of biological replicates (n=3, error bars show standard deviation. Expression of eGFP fusions from P_{xylX} was induced with 0.1 % xylose.

The N-terminal extremity of ChvG determines localisation and relocation

ChvG is a HK anchored in the membrane thanks to 2 transmembrane helices which delimit a periplasmic sensor domain (amino acids 50-221), with a cytoplasmic signal transduction histidine kinase domain (amino acids 242-534) (Fig. 7A). To assess which of these ChvG domains are essential for localisation, we fused to mCherry ChvG versions harbouring either the complete or truncated sensor ($ChvG_{1-274}$ and $ChvG_{1-114}$, respectively) or the catalytic ($ChvG_{273-534}$) domain. First, we confirmed that full-length ChvG fused to mCherry displayed the same localisation and relocation patterns (Fig. 7B, F) than the ones described for GFP fusions (Fig. 6A). Interestingly, the truncated or complete sensor domain alone ($ChvG_{1-114}$, $ChvG_{1-274}$) fused to mCherry were both localized as patchy-spotty in PYE (Fig. 7C-D). However, only the $ChvG_{1-274}$-mCherry fusion relocated as foci upon transition to M2G (Fig. 7G-H). Unlike the sensor domains, the catalytic domain ($ChvG_{273-534}$) fused to mCherry displayed neither the patchy-spotty nor the foci pattern of localization and was instead diffusely localized in the cytoplasm (Fig. 7E, I). Altogether, our results indicate that the complete periplasmic sensor domain of ChvG edged by transmembrane domains are required for relocation as foci upon osmotic shock whereas the first 114 amino acids are sufficient to determine the patchy-spotty pattern of localization.

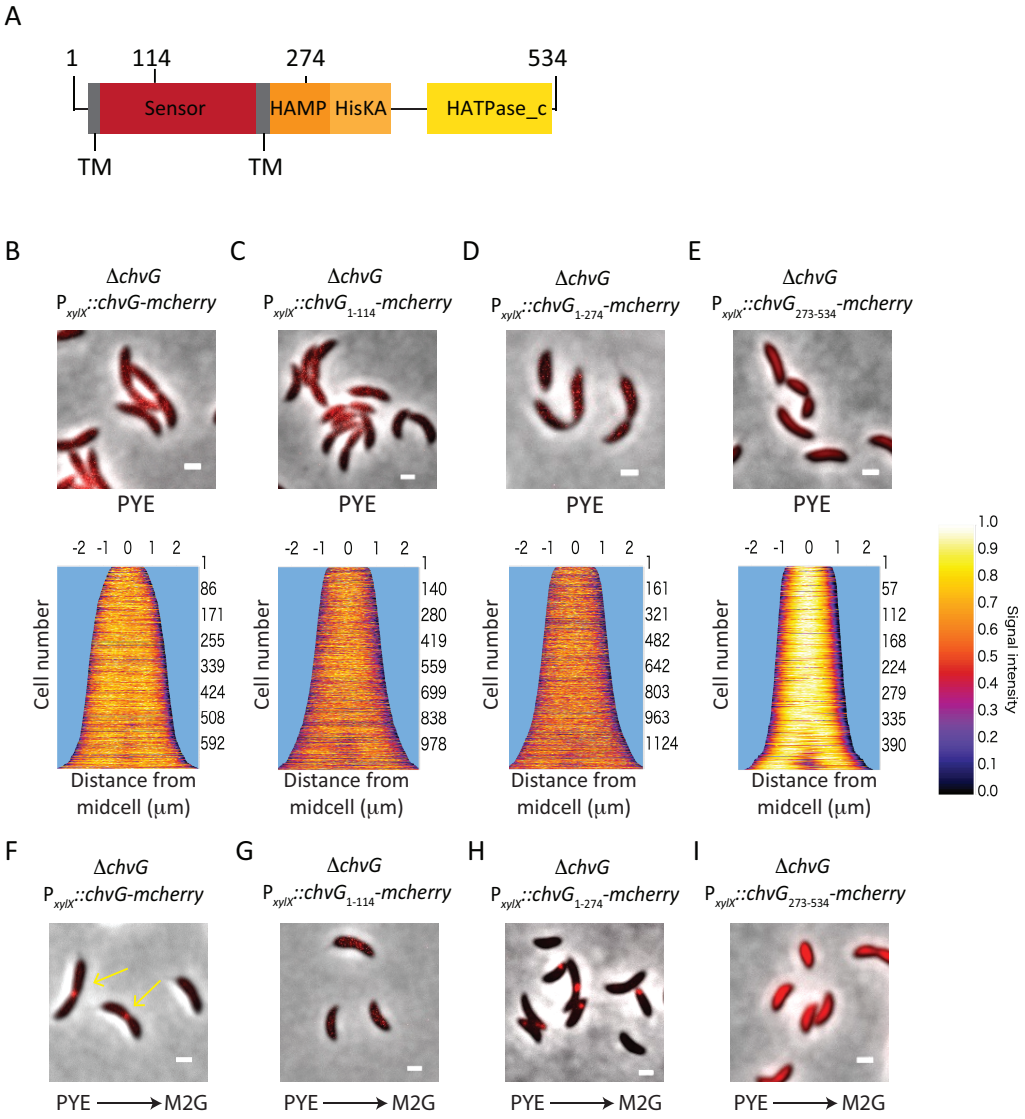

Fig. 7. Localisation of truncated ChvG variants. (A) Conserved domains in the HK ChvG and position of the amino acids defining the truncated proteins. (B-I) Localisation of ChvG WT (B, F) and truncated versions (C-E, G-I) in cells grown in PYE and imaged on PYE agarose pads (B-) or in cells grown in PYE, washed in M2G and imaged on M2G agarose pads (PYE → M2G) (F-I). Liquid cultures and pads were supplemented with 0.1 % xylose. Scale bars in microscopy images correspond to 1 μm.

Discussion

The α-proteobacterial TCS ChvGI has conserved cell envelope regulatory functions (Lamontagne *et al.*, 2007; Heckel *et* al., 2014; Ratib *et al.*, 2018; Vallet *et al.*, 2020; Stein *et al.*, 2021), but the exact perceived signal that triggers the ChvG-dependent phosphorylation of ChvI remains unknown. We found that hyperosmotic shock triggers ChvI phosphorylation and treatment with antibiotics targeting PG synthesis proteins induces *chvIG* expression. We also showed that ChvI regulates expression of genes related to PG synthesis, such as *ftsN* and *dipM*, and to osmotic and oxidative stress regulation, such as *nepR*, likely explaining why ChvGI system is required for viability in these stressful conditions. Other targets related to cell envelope architecture, identified by ChIP-seq and RNA-seq experiments, include genes coding for the β-barrel assembly machinery (Bam) complex; components of the Tol system; several outer membrane proteins (OMP) such as RasFa, CCNA_03820 and CCNA_01956; and the cytoplasmic FtsZ-binding protein ZapA. Altogether, our results support a role for ChvGI in *C. crescentus* as a safeguard of cell envelope homeostasis by sensing cell wall-related damages and regulating the expression of genes related to cell division and envelope architecture.

We observed that similarly to Δ*chvI*, the endogenous expression of phospho-mimetic (*chvI*$_{D52E}$) or phospho-ablative (*chvI*$_{D52A}$) failed to grow in hypertonic conditions such as those found in synthetic minimal media (M2G or M2X). However, ectopic expression of *chvI*$_{D52E}$ partially alleviated growth defect of Δ*chvI* in these conditions, in agreement with a previous report (Stein *et al.* (2021). These observations indicate that ChvI phosphorylation dynamics is tightly regulated to ensure optimal growth of *C. crescentus* in hyperosmotic environments. Therefore, an important level of

563 phosphorylated ChvI might be required even in mild cell envelope stress conditions.
564 In addition, constitutive activation of a cell envelope stress response system can be
565 detrimental, as already shown in *E. coli* with the sigma factor E (σ^E), the inner
566 membrane stress regulator Cpx or the regulator of capsule synthesis Rcs (Missiakas
567 *et al*., 1997; Pogliano *et al*., 1998; De las Peñas *et al*., 2003; Grabowicz & Silhavy.
568 2017), Indeed, overactivation of σ^E causes overexpression of sRNAs inhibiting
569 expression of integral OMPs, therefore weakening the outer membrane integrity
570 (Nicoloff *et al*., 2017). Likewise, constitutive Cpx activation disturbs cell division and
571 morphology causing mis-localisation of FtsZ as well as overexpression of L,D-
572 transpeptidase enzyme LdtD (Pogliano *et al*., 1998; Delhaye *et al.,* 2016). Similarly,
573 overactivation of the RR RcsB results in overexpression of the small outer membrane
574 lipoprotein OsmB, which is toxic through yet unknown mechanisms (Grabowicz &
575 Silhavy. 2017). In any of the previous cases, hyperstimulation can lead to deregulation
576 of cell envelope components.
577 In *C. crescentus*, the general stress response (GSR) sigma factor SigT is also
578 activated upon osmotic imbalance thanks to a complex network comprising the sRNA
579 (GsrN), the anti-SigT regulator (NepR), the histidine phosphotransferases (LovK and
580 PhyK) and the response regulators (MrrA, LovR and PhyR) (Alvarez-Martinez *et al*.,
581 2007; Lourenço *et al*., 2011; Foreman *et al*., 2012; Lori *et al*., 2018; Tien *et al*., 2018).
582 In steady-state conditions, NepR impedes SigT-dependent transcription. Upon either
583 oxidative stress or osmotic imbalance, the histidine phosphotransferase MrrA
584 activates PhyK to further phosphorylate PhyR. Once phosphorylated, PhyR~P
585 interacts with NepR to release SigT from inhibition and allow the expression the SigT-
586 dependent regulon. Interestingly, we found that ChvIG and GSR are interconnected

but this connection is counterintuitive. Indeed, we observed (i) that deletion of *sigT* led to higher *chvI* promoter activity and (ii) that ChvI directly represses *phyR* expression, suggesting that ChvI and SigT antagonise each other despite being sensitive to hyperosmotic conditions. However, we cannot exclude the possibility that the cell envelope homeostasis is sufficiently disrupted in both single mutants to correspondingly activate the other functional system, *i.e.* ChvGI in Δ*sigT* through P_{chvIG} and SigT in Δ*chvI* through P_{phyR}. Alternatively, the antagonistic regulation might allow these two systems to respond to different levels of osmotic imbalances. For instance, activation of ChvGI at low hypertonic conditions could down-regulate GSR whereas SigT would be sensitive to higher salts concentrations at which ChvGI would be tuned down.

In the absence of a functional ChvGI system, *C. crescentus* cannot propagate in minimal media except if the TonB-dependent outer membrane protein ChvT or if NtrX is concomitantly inactivated (Stein *et al.,* 2021). ChvGI is known to indirectly down-regulate ChvT by directly activating the expression of the sRNA ChvR (Fröhlich *et al*., 2018). Our ChIP-seq data showed that ChvI also likely regulates *chvT* expression directly by binding to its promoter region. This dual – transcriptional and post-transcriptional – control indicates the ChvT outer membrane protein is an important player in cell envelope homeostasis. In support of that, a Δ*chvI* Δ*chvT* double mutant grew better than a Δ*chvI* single one in hyperosmotic regimes. Interestingly, NtrXY has been also described as a cell envelope regulator in α-proteobacteria. NtrYX controls succinoglycan and exopolysaccharide (EPS) production, and salt stress response in *S. meliloti* (Wang *et al*., 2013; Calatrava *et al*., 2017). In *Rhodobacter sphaeroides,* NtrXY confers resistance to membrane disruptive agents and regulates the expression

611 of genes coding for PG and EPS synthesis enzymes, lipoproteins and cell division
612 proteins (Lemmer *et al.,* 2017; Lemmer *et al*., 2020). Thus, confirming that *ntrX*
613 inactivation in a Δ*chvI* background partially restored growth in the presence of high
614 concentration of osmolytes further supports the importance of the NtrZXY system,
615 together with ChvGI, in the cell envelope stress response in α-proteobacteria.
616 We showed that ChvGI also regulates sensitivity to the antibiotic mecillinam that
617 inhibits PG transpeptidation. Previously, Vallet *et al*. (2020) showed that *chvI* mutants
618 failed to grow when exposed to vancomycin, which also impedes PG crosslinking by
619 directly interacting with the D-Ala-D-Ala moiety of the PG precursors. Here, we showed
620 that Δ*chvI* cells were sensitized to mecillinam and to a lesser extent to vancomycin.
621 However, although both antibiotics inhibits the transpeptidation step of PG synthesis,
622 only mecillinam treatment induced *chvIG* expression. This is likely due to the fact that
623 intracellular concentrations of vancomycin remain low in WT cells since the TonB-
624 dependent receptor ChvT is poorly expressed and incorporated in outer membrane.
625 However, treatment with cefixime, cefotaxime and sodium deoxycholate did not show
626 differences in cell viability between WT and Δ*chvI* cells (Vallet *et al*. 2020).
627 Furthermore, the activation of *chvR* expression upon cefotaxime or sodium
628 deoxycholate exposure was shown to be ChvI-independent. In addition, we showed
629 here that Δ*chvI* cells were not more sensitive to treatment with SDS, polymyxin B or
630 the MreB inhibitor A22. Considering that MreB is a key cytoplasmic component of the
631 elongasome complex, of which PBP2 and other proteins are part, it is therefore likely
632 that ChvGI rather senses specific targets in the periplasm to assess cell envelope
633 stress. Notwithstanding that, other stress response systems, yet to be discovered or

634 characterised in the context of the aforementioned stressors, might be involved in
635 responding to the damages that do not activate ChvGI.
636 We observed that ChvG has a patchy-spotty pattern localisation when grown in
637 complex and synthetic minimal media, while it relocates as foci at mid-cell upon
638 transition from complex to minimal media. The patchy-spotty localisation pattern has
639 been described for multiple PG-related proteins in *C. crescentus*, including MreB,
640 MreC, Pal, PBP1A, PBP2, RodA, TolB (Figge *et* al., 2004; Divakaruni *et al.,* 2005;
641 Werner *et al*., 2009; Hocking *et al.,* 2012; Billini *et al*., 2019). Moreover, RodA, PBP2,
642 PBP1A, which are proteins involved in PG polymerization and crosslinking, have been
643 reported to relocate at mid-cell upon osmotic upshift in a FtsZ-dependent but MreB-
644 independent manner (Hocking *et al.,* 2012). It would be interesting to check whether
645 this ChvG localisation patterns are conserved among α-proteobacteria, in particular in
646 Rhizobiales since they do not encode MreB orthologs. In *E. coli*, it has been reported
647 that the PBP2 periplasmic portion physically interacts with those of PBP1A and RodA
648 to mediate PG assembly and to ensure proper cell elongation (Banzhaf *et al*., 2012;
649 van der Ploeg *et al*., 2015). It is yet to determine whether ChvG interacts with PBP2,
650 PBP1a, RodA and/or others with similar localisation patterns. Nonetheless, it is
651 tempting to speculate that ChvG interacts and co-localises with PG-related enzymes
652 as a cell envelope safeguard system in α-proteobacteria. A recent study in the Gram-
653 positive bacterium *Bacillus thuringiensis* showed that upon treatment with the
654 antibiotic cefoxitin, the putative PBP protein PbpP derepresses the extracytoplasmic
655 function sigma factor P (σ^P) which increases resistance to β-lactams (Nauta *et al*.,
656 2021). Future experiments will aim to determine the ChvG interactome under cell
657 envelope undisturbed and threatening conditions, and dissect its activation

658 mechanism as well as its connection with the general stress response, not only in *C.*
659 *crescentus* but also in other α-proteobacteria.
660

661 ## Acknowledgments

662 We are grateful to Clare Kirkpatrick, Sean Crosson and Benjamin Stein for willingness
663 to discuss and share data on their ChvGI-related projects. Also, we would like to thank
664 members of the URBM of the University of Namur for their comments and suggestions
665 on this project, especially Dr. Angéline Reboul from her comments and advices on the
666 microscopy analysis. This work was supported by the Fonds de la Recherche
667 Scientifique – FNRS (F.R.S. – FNRS) with a Welbio Starting Grant (WELBIO-CR-
668 2019S-05) to R.H. A.Q-Y. was supported by a postdoctoral fellowship from the
669 University of Namur (UNamur). R.H. is a Research Associate of F.R.S. – FNRS.
670

671 ## Author Contributions

672 A.Q-Y. and R.H. conceived and designed the experiments. A.Q-Y. performed all the
673 experiments except otherwise stated. A.M. purified the ChvI protein and helped with
674 some plasmids constructs. A.Q-Y., J.C. and R.H. analyzed the data. A.Q-Y. and R.H.
675 wrote the paper.
676

677 ## Competing financial interests

678 The authors declare no competing financial interests.
679

References

Afgan, E., Baker, D., Batut, B., Van Den Beek, M., Bouvier, D., Čech, M., ... & Blankenberg, D. (2018). The Galaxy platform for accessible, reproducible and collaborative biomedical analyses: 2018 update. *Nucleic acids research*, *46*(W1), W537-W544.

Altamirano-Silva, P., Meza-Torres, J., Castillo-Zeledón, A., Ruiz-Villalobos, N., Zuñiga-Pereira, A. M., Chacón-Díaz, C., … & Chaves-Olarte, E. (2018). *Brucella abortus* senses the intracellular environment through the BvrR/BvrS two-component system, which allows B. abortus to adapt to its replicative niche. *Infection and immunity*, *86*(4), e00713-17.

Alvarez-Martinez, C. E., Lourenço, R. F., Baldini, R. L., Laub, M. T., & Gomes, S. L. (2007). The ECF sigma factor σT is involved in osmotic and oxidative stress responses in *Caulobacter crescentus*. *Molecular microbiology*, *66*(5), 1240-1255.

Banzhaf, M., van den Berg van Saparoea, B., Terrak, M., Fraipont, C., Egan, A., Philippe, J., ... & Vollmer, W. (2012). Cooperativity of peptidoglycan synthases active in bacterial cell elongation. *Molecular microbiology*, *85*(1), 179-194.

Billini, M., Biboy, J., Kühn, J., Vollmer, W., & Thanbichler, M. (2019). A specialized MreB-dependent cell wall biosynthetic complex mediates the formation of stalk-specific peptidoglycan in *Caulobacter crescentus*. *PLoS genetics*, *15*(2), e1007897.

Calatrava-Morales, N., Nogales, J., Ameztoy, K., van Steenbergen, B., & Soto, M. J. (2017). The NtrY/NtrX system of *Sinorhizobium meliloti* GR4 regulates motility, EPS I production, and nitrogen metabolism but is dispensable for symbiotic nitrogen fixation. *Molecular Plant-Microbe Interactions*, *30*(7), 566-577.

Capra, E. J., & Laub, M. T. (2012). Evolution of two-component signal transduction systems. *Annual review of microbiology*, *66*, 325-347.

Carrica, M. D. C., Fernandez, I., Martí, M. A., Paris, G., & Goldbaum, F. A. (2012). The NtrY/X two-component system of *Brucella* spp. acts as a redox sensor and regulates the expression of nitrogen respiration enzymes. *Molecular microbiology*, *85*(1), 39-50.

Chen, E. J., Sabio, E. A., & Long, S. R. (2008). The periplasmic regulator ExoR inhibits ExoS/ChvI two-component signalling in *Sinorhizobium meliloti*. *Molecular microbiology*, *69*(5), 1290-1303.

Cho, S. H., Szewczyk, J., Pesavento, C., Zietek, M., Banzhaf, M., Roszczenko, P., ... & Collet, J. F. (2014). Detecting envelope stress by monitoring β-barrel assembly. *Cell*, *159*(7), 1652-1664.

Christen, M., Beusch, C., Bösch, Y., Cerletti, D., Flores-Tinoco, C. E., Del Medico, L., ... & Christen, B. (2016). Quantitative selection analysis of bacteriophage ϕCbK

susceptibility in *Caulobacter crescentus*. *Journal of molecular biology*, *428*(2), 419-430.

De Las Peñas, A., Connolly, L., & Gross, C. A. (1997). The σE-mediated response to extracytoplasmic stress in *Escherichia coli* is transduced by RseA and RseB, two negative regulators of σ^E. *Molecular microbiology*, *24*(2), 373-385.

Delhaye, A., Collet, J. F., & Laloux, G. (2016). Fine-tuning of the Cpx envelope stress response is required for cell wall homeostasis *in Escherichia coli*. *MBio*, *7*(1), e00047-16.

Divakaruni, A. V., Loo, R. R. O., Xie, Y., Loo, J. A., & Gober, J. W. (2005). The cell-shape protein MreC interacts with extracytoplasmic proteins including cell wall assembly complexes in *Caulobacter crescentus*. *Proceedings of the National Academy of Sciences*, *102*(51), 18602-18607.

Ducret, A., Quardokus, E. M., & Brun, Y. V. (2016). MicrobeJ, a tool for high throughput bacterial cell detection and quantitative analysis. *Nature Microbioly* 1: 16077.

Figge, R. M., Divakaruni, A. V., & Gober, J. W. (2004). MreB, the cell shape-determining bacterial actin homologue, co-ordinates cell wall morphogenesis in *Caulobacter crescentus*. *Molecular microbiology*, *51*(5), 1321-1332.

Foreman, R., Fiebig, A., & Crosson, S. (2012). The LovK-LovR two-component system is a regulator of the general stress pathway in *Caulobacter crescentus*. *Journal of bacteriology*, *194*(12), 3038-3049.

Gao, R., & Stock, A. M. (2009). Biological insights from structures of two-component proteins. *Annual review of microbiology*, *63*, 133-154

Geiger, O., Sohlenkamp, C., Vera-Cruz, D., Medeot, D. B., Martínez-Aguilar, L., Sahonero-Canavesi, D. X., ... & López-Lara, I. M. (2021). ExoS/ChvI two-component signal-transduction system activated in the absence of bacterial phosphatidylcholine. *Frontiers in plant science*, *12*.

Goulian, M. (2010). Two-component signaling circuit structure and properties. *Current opinion in microbiology*, *13*(2), 184-189.

Grabowicz, M., & Silhavy, T. J. (2017). Redefining the essential trafficking pathway for outer membrane lipoproteins. *Proceedings of the National Academy of Sciences*, *114*(18), 4769-4774

Heckel, B. C., Tomlinson, A. D., Morton, E. R., Choi, J. H., & Fuqua, C. (2014). *Agrobacterium tumefaciens exoR* controls acid response genes and impacts exopolysaccharide synthesis, horizontal gene transfer, and virulence gene expression. *Journal of bacteriology*, *196*(18), 3221-3233.

Hocking, J., Priyadarshini, R., Takacs, C. N., Costa, T., Dye, N. A., Shapiro, L., ... & Jacobs-Wagner, C. (2012). Osmolality-dependent relocation of penicillin-binding protein PBP2 to the division site in *Caulobacter crescentus*. *Journal of bacteriology*, *194*(12), 3116-3127.

Huynh, T. N., & Stewart, V. (2011). Negative control in two-component signal transduction by transmitter phosphatase activity. *Molecular microbiology*, *82*(2), 275-286.

Jubelin, G., Vianney, A., Beloin, C., Ghigo, J. M., Lazzaroni, J. C., Lejeune, P., & Dorel, C. (2005). CpxR/OmpR interplay regulates curli gene expression in response to osmolarity in *Escherichia coli. Journal of bacteriology*, *187*(6), 2038-2049.

Lamontagne, J., Butler, H., Chaves-Olarte, E., Hunter, J., Schirm, M., Paquet, C., ... & Paramithiotis, E. (2007). Extensive cell envelope modulation is associated with virulence in *Brucella abortus*. *Journal of proteome research*, *6*(4), 1519-1529.

Laubacher, M. E., & Ades, S. E. (2008). The Rcs phosphorelay is a cell envelope stress response activated by peptidoglycan stress and contributes to intrinsic antibiotic resistance. *Journal of bacteriology*, *190*(6), 2065-2074.

Lemmer, K. C., Alberge, F., Myers, K. S., Dohnalkova, A. C., Schaub, R. E., Lenz, J. D., ... & Donohue, T. J. (2020). The NtrYX two-component system regulates the bacterial cell envelope. *Mbio*, *11*(3), e00957-20.

Lemmer, K. C., Zhang, W., Langer, S. J., Dohnalkova, A. C., Hu, D., Lemke, R. A., ... & Donohue, T. J. (2017). Mutations that alter the bacterial cell envelope increase lipid production. *Mbio*, *8*(3), e00513-17.

Li, L., Jia, Y., Hou, Q., Charles, T. C., Nester, E. W., & Pan, S. Q. (2002). A global pH sensor: *Agrobacterium* sensor protein ChvG regulates acid-inducible genes on its two chromosomes and Ti plasmid. *Proceedings of the National Academy of Sciences*, *99*(19), 12369-12374.

Lori, C., Kaczmarczyk, A., de Jong, I., & Jenal, U. (2018). A single-domain response regulator functions as an integrating hub to coordinate general stress response and development in Alphaproteobacteria. *MBio*, *9*(3), e00809-18.

Lourenço, R. F., Kohler, C., & Gomes, S. L. (2011). A two-component system, an anti-sigma factor and two paralogous ECF sigma factors are involved in the control of general stress response in *Caulobacter crescentus*. *Molecular microbiology*, *80*(6), 1598-1612.

Mantis, N. J., & Winans, S. C. (1993). The chromosomal response regulatory gene chvI of *Agrobacterium tumefaciens* complements an *Escherichia coli* phoB mutation and is required for virulence. *Journal of bacteriology*, *175*(20), 6626-6636.

Mirabella, A., Terwagne, M., Zygmunt, M. S., Cloeckaert, A., De Bolle, X., & Letesson, J. J. (2013). *Brucella melitensis* MucR, an orthologue of Sinorhizobium meliloti MucR, is involved in resistance to oxidative, detergent, and saline stresses and cell envelope modifications. *Journal of bacteriology*, *195*(3), 453-465.

Missiakas, D., Mayer, M. P., Lemaire, M., Georgopoulos, C., & Raina, S. (1997). Modulation of the *Escherichia coli* σ^E (RpoE) heat-shock transcription-factor activity by the RseA, RseB and RseC proteins. *Molecular microbiology*, *24*(2), 355-371.

Nauta, K. M., Ho, T. D., & Ellermeier, C. D. (2021). The Penicillin-Binding Protein PbpP Is a Sensor of β-Lactams and Is Required for Activation of the Extracytoplasmic Function σ Factor σ^P in *Bacillus thuringiensis*. *Mbio*, *12*(2), e00179-21.

Nicoloff, H., Gopalkrishnan, S., & Ades, S. E. (2017). Appropriate regulation of the σ^E-dependent envelope stress response is necessary to maintain cell envelope integrity and stationary-phase survival in *Escherichia coli. Journal of bacteriology*, *199*(12), e00089-17.

Pawlowski, K., Klosse, U., & De Bruijn, F. J. (1991). Characterization of a novel *Azorhizobium caulinodans* ORS571 two-component regulatory system, NtrY/NtrX, involved in nitrogen fixation and metabolism. *Molecular and General Genetics MGG*, *231*(1), 124-138.

Pini, F., De Nisco, N. J., Ferri, L., Penterman, J., Fioravanti, A., Brilli, M., ... & Biondi, E. G. (2015). Cell cycle control by the master regulator CtrA in *Sinorhizobium meliloti*. *PLoS genetics*, *11*(5), e1005232.

Pogliano, J., Dong, J. M., De Wulf, P., Furlong, D., Boyd, D., Losick, R., ... & Lin, E. C. C. (1998). Aberrant cell division and random FtsZ ring positioning in *Escherichia coli cpxA** mutants. *Journal of bacteriology*, *180*(13), 3486-3490.

Raivio, T. L., & Silhavy, T. J. (1997). Transduction of envelope stress *in Escherichia coli* by the Cpx two-component system. *Journal of bacteriology*, *179*(24), 7724-7733.

Ratib, N. R., Sabio, E. Y., Mendoza, C., Barnett, M. J., Clover, S. B., Ortega, J. A., ... & Chen, E. J. (2018). Genome-wide identification of genes directly regulated by ChvI and a consensus sequence for ChvI binding in *Sinorhizobium meliloti*. *Molecular microbiology*, *110*(4), 596-615.

Stein, B. J., Fiebig, A., & Crosson, S. (2021). The ChvG–ChvI and NtrY–NtrX two-component systems coordinately regulate growth of *Caulobacter crescentus*. *Journal of Bacteriology*, JB-00199.

Stock, A. M., Robinson, V. L., & Goudreau, P. N. (2000). Two-component signal transduction. *Annual review of biochemistry*, *69*(1), 183-215.

Thanbichler, M., & Shapiro, L. (2006). MipZ, a spatial regulator coordinating chromosome segregation with cell division in *Caulobacter*. *Cell*, *126*(1), 147-162.

Thanbichler, M., Iniesta, A. A., & Shapiro, L. (2007). A comprehensive set of plasmids for vanillate-and xylose-inducible gene expression in *Caulobacter crescentus*. *Nucleic acids research*, *35*(20), e137-e137.

Tien, M. Z., Stein, B. J., & Crosson, S. (2018). Coherent feedforward regulation of gene expression by Caulobacter σ^T and GsrN during hyperosmotic stress. *Journal of bacteriology*, *200*(19), e00349-18.

Vallet, S. U., Hansen, L. H., Bistrup, F. C., Laursen, S. A., Chapalay, J. B., Chambon, M., ... & Kirkpatrick, C. L. (2020). Loss of bacterial cell pole stabilization in *caulobacter crescentus* sensitizes to outer membrane stress and peptidoglycan-directed antibiotics. *Mbio*, *11*(3), e00538-20.

Van der Ploeg, R., Goudelis, S. T., & Den Blaauwen, T. (2015). Validation of FRET assay for the screening of growth inhibitors of *Escherichia coli* reveals elongasome assembly dynamics. *International journal of molecular sciences*, *16*(8), 17637-17654.

Wang, D., Xue, H., Wang, Y., Yin, R., Xie, F., & Luo, L. (2013). The *Sinorhizobium meliloti ntrX* gene is involved in succinoglycan production, motility, and symbiotic nodulation on alfalfa. *Applied and environmental microbiology*, *79*(23), 7150-7159.

Werner, J. N., Chen, E. Y., Guberman, J. M., Zippilli, A. R., Irgon, J. J., & Gitai, Z. (2009). Quantitative genome-scale analysis of protein localization in an asymmetric bacterium. *Proceedings of the National Academy of Sciences*, *106*(19), 7858-7863

Wu, C. F., Lin, J. S., Shaw, G. C., & Lai, E. M. (2012). Acid-induced type VI secretion system is regulated by ExoR-ChvG/ChvI signaling cascade in Agrobacterium tumefaciens. *PLoS Pathog.* 8, e1002938